JOURNAL OF SPACECRAFT AND ROCKETS
Vol. 32, No. 3, May–June 1995

Engineering Notes

ENGINEERING NOTES are short manuscripts describing new developments or important results of a preliminary nature. These Notes cannot exceed 6 manuscript pages and 3 figures; a page of text may be substituted for a figure and vice versa. After informal review by the editors, they may be published within a few months of the date of receipt. Style requirements are the same as for regular contributions (see inside back cover).

Aerodynamic Heating to Spherically Blunted Cones at Angle of Attack

Jason P. Shimshi*
The Aerospace Corporation,
El Segundo, California 90245-4691
and
Gerald D. Walberg†
North Carolina State University,
Raleigh, North Carolina 27695

Nomenclature

d = diameter
$H_{t,1}$ = enthalpy of tunnel reservoir
H_w = enthalpy of outer wall of tunnel model
h = heat transfer coefficient, W · kg/J · m^2
h_{FR} = Fay–Riddell value of the heat transfer coefficient, W· kg/J · m^2
$\dot{q}_{FR}$ = Fay–Riddell value of the heat transfer rate, W/m^2
R_b = base radius of model
R_c = corner radius of model
R_n = nose radius of model
Re_∞ = unit Reynolds number, ft^{-1}
S = running length (from center of spherical nose)
α = angle of attack, deg
θ_c = cone half angle, deg

Introduction

RECENTLY, a great deal of effort has been expended to examine aerobraking and aerocapture technologies. Aerobraking, which is defined as using a planet's atmosphere to decelerate upon entry, has been shown to yield significant savings in the propellant required for a mission, allowing a larger payload to be installed. It also has been shown that vehicles can use a planet's atmosphere to change their orbital characteristics. Various shapes considered for use as aeroassisted space transfer vehicles, or ASTVs, and aerobrakes include biconics (axisymmetric and bent), raked cones, axisymmetric cones, and Aeroassist Flight Experiment (AFE) shapes.

A study has been conducted to examine the effects of geometry and angle of attack on the aerodynamic heating to potential ASTVs as well as to examine the effectiveness of two methods used in the preliminary design stage to predict the convective heat transfer to potential ASTVs. In order to examine generic ASTVs, two spherically blunted, wide-angle cones are considered. These cones have half angles of $\theta_c = 50$ and 70 deg, a nose-to-base radius ratio (R_n/R_b) of 0.5, and a corner-to-base radius ratio (R_c/R_b) of 0.125.

Received June 28, 1994; revision received Nov. 1, 1994; accepted for publication Nov. 11, 1994.

*Member of the Technical Staff, Flight Mechanics Department. Member AIAA.
†Professor of Mechanical and Aerospace Engineering. Fellow AIAA.

Comparisons were made with results from two axisymmetric analog boundary-layer solutions. The comparisons will allow an estimation of the boundary-layer solutions' ability to predict the heating to ASTVs in preliminary design analysis.

Experimental and Computational Methods

The experimental data in this study were obtained in NASA-Langley's 15-in. and 20-in. Mach 6 tunnels, which are described in Refs. 1 and 2, from tests conducted by N. M. Reddy and C. G. Miller in 1986 and the authors in 1992. The experimental data examine the heating to both the leeward and windward centerlines. These tests and the wind-tunnel models used have been documented in Refs. 3 and 4.

An uncertainty analysis for thin-skin thermocouple data, as shown in Ref. 3, results in an experimental error of 12%.

To provide flowfield characteristics and streamline patterns for the axisymmetric analog boundary-layer technique, the computer code HALIS (High Alpha Inviscid Solution) was used. Originally developed for Shuttle-like vehicles with large embedded subsonic regions in their flowfields, HALIS solves for the flowfield over blunt bodies in ideal air by integrating the time-dependent, three-dimensional, compressible Euler equations. The solution of the blunt-body problem and the specific method and equations used by HALIS are discussed in Ref. 5. Each cone grid is equipped with a cylindrical extension to provide the required supersonic outflow boundary. The details of the grid generation for the wide-angle cones are discussed in Ref. 4 and are similar to the methods used in Ref. 6.

The axisymmetric analog method, originally developed by Cooke,[7] was used to obtain predicted heating rates over the blunted sphere cones at angle of attack. Briefly, this method takes the three-dimensional boundary-layer equations and, by writing them in a streamline coordinate system and neglecting the crossflow velocity in the boundary layer, is able to reduce them to their axisymmetric form. In this form, the metric of the streamline spreading is interpreted as the radius of the equivalent axisymmetric body, and any algorithm capable of predicting the heating to axisymmetric bodies can be used. In this study, two axisymmetric boundary-layer codes calculated the heating rate along the inviscid centerline streamlines from the stagnation point using the flowfield data from HALIS.

The two axisymmetric analog boundary-layer codes use separate methods to calculate the heating rate. AA3DBL uses a method developed by Zoby et al.[8] to calculate laminar surface heating rates. SABLE[9] solves the nonsimilar boundary-layer equations over an axisymmetric body. Since AA3DBL uses an approximate integral boundary-layer correlation and SABLE a nonsimilar solution, the differences between the two codes will reflect the nonsimilarity of the boundary layer as well as the effectiveness of the Zoby–Moss–Sutton[8] algorithm used in AA3DBL.

As used in this study, both computational methods have the built-in assumption of constant wall temperature. By presenting the results in the form of a normalized heat transfer coefficient, h/h_{FR}, where $h_{FR} = \dot{q}_{FR}/(H_{t,1} - H_w)$ and $\dot{q}_{FR}$ is the heat transfer coefficient as calculated by Fay and Riddell,[10] the effects of varying wall temperature should be minimized.

Results

The effects of varying α have been documented in previous studies, such as Ref. 6. Figures 1 and 2 show h/h_{FR} vs S/R_b for the 50-

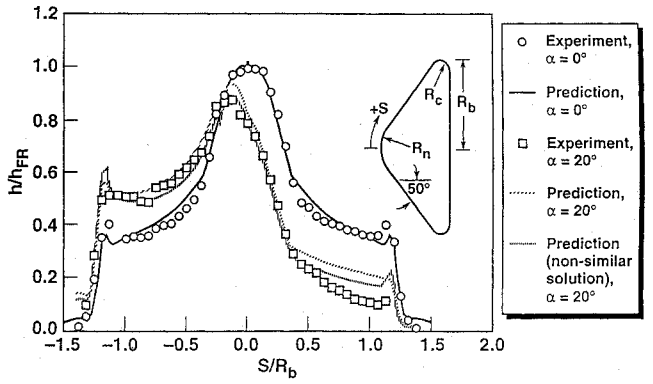

Fig. 1 Heat transfer distribution to the 50-deg cone centerline at $\alpha = 0$ and 20 deg.

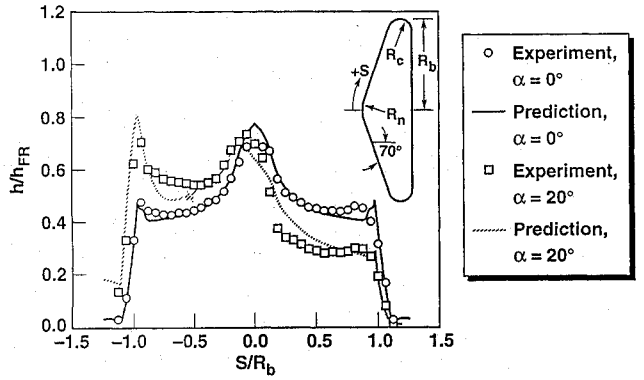

Fig. 2 Heat transfer distribution to the 70-deg cone centerline at $\alpha = 0$ and 20 deg.

and 70-deg sphere cones, respectively, at $\alpha = 0$ deg and $\alpha = 20$ deg. By examining the experimental data, several trends are apparent. There are three heating peaks: one at the nose of the cone ($S/R_b = 0$) and one each at the leeward and windward corners. As α increases, the heating increases over the windward cone flank and decreases over the leeward cone flank. As the cone angle increases, the flow's acceleration along both cone flanks decreases, increasing the expansion of the flow around the corners and hence the heating rate as well. In addition, the heating at the nose decreases from the Fay–Riddell value. One other effect is notable: the maximum heating does not necessarily coincide with the stagnation region. The windward centerline of a 70-deg cone at $\alpha = 20$ deg will be normal to the flow, resulting in the presence of a stagnation region approximately halfway down the cone flank. Since the flow cannot accelerate along the windward centerline, it must accelerate rapidly around the nose and corner, providing larger heating rates at those locations than at the stagnation point.

Examining the predicted results, it was noted that AA3DBL and SABLE produced similar results, as shown in Fig. 1 for the 50-deg cone at $\alpha = 20$ deg, implying that the nonsimilarity of the boundary layer is not an issue. Hence, only AA3DBL results will be shown for the other cases.

The predicted results for both the 50- and 70-deg cones compare very well with the experimental results at $\alpha = 0$ deg. However, at $\alpha = 20$ deg the comparison is not as good, particularly on both cone flanks of the 70-deg cone and the leeside cone flank ($S/R_b > 0$) of the 50-deg cone. The heating on the windward corner of the 70-deg cone is predicted well, but because of the discrete nature of the experimental results, it is unclear if the heating is as large as AA3DBL predicts.

The discrepancies could result from one of two possibilities. First, the inviscid solution from HALIS may be the cause, possibly through an unexpected sensitivity of the solution to the flowfield grid. Second, the discrepancies may have resulted from the assumption of a decoupled inviscid solution and boundary layer, which may break down on the leeside of the 50-deg cone at angle of attack.

Concluding Remarks

Heat transfer distributions were measured on the forebody centerlines of 50- and 70-deg-half-angle, spherically blunted cone models. The effect of angle of attack and cone half angle were examined. Predictions of the inviscid flowfield were obtained from HALIS and used as boundary-layer edge conditions for two axisymmetric analog boundary-layer algorithms, one using an approximate integral boundary-layer correlation and the other solving the nonsimilar boundary-layer equations, which provided predictions of heat transfer.

The effect of increasing the cone half angle is to decrease the heating to the nose and increase the heating to the corners. As the angle of attack was increased, the heat transfer to the windward side increased while the leeside heating decreased. In addition, the stagnation region and region of peak heating did not necessarily coincide at angle of attack. The peak heating was concentrated in regions of flow expansion, i.e., the corners and spherical nose. For the 70-deg cones at large angle of attack, the heating at the windward corner was comparable to the heating at the nose. This implies that the heating at the windward corner should be considered, as well as the nose, if these shapes are to be used as ASTVs.

The two computational methods used did not show a significant difference, implying that the nonsimilarity of the boundary layer is not an issue. The predicted results compared well with the experimental results at $\alpha = 0$ deg. However, at $\alpha = 20$ deg, discrepancies were noted on the leeside of the 50-deg cone and on the leeside and windward cone flanks of the 70-deg cone. This implies that either the solution for the flowfield at angle of attack is suspect or the assumption of a decoupled boundary layer and inviscid flowfield is not appropriate. The causes of these observed discrepancies represent potentially fruitful areas for further research.

Acknowledgments

This study was conducted to partially fulfill the requirements of the Master of Science degree at the George Washington University for the first author. The authors wish to thank Charles Miller of Langley Research Center for his assistance and his permission to use previously unpublished data in this study, and Dr. Reddy for that unpublished data set. The authors also wish to thank the National Aeronautics and Space Administration and Langley Research Center for use of their facilities during this study, as well as the members of the Experimental Hypersonics Branch and Harris Hamilton and Jim Weilmuenster of the Space Systems Division at Langley for their assistance.

References

[1]Hodge, J. S., "The Langley 15-Inch Mach 6 High Temperature Tunnel," AIAA Paper 92-3938, July 1992.

[2]Miller, C. G., "Langley Hypersonic Aerodynamic/Aerothermodynamic Testing Capabilities—Present and Future," AIAA Paper 90-1376, June 1990.

[3]Shimshi, J. P., "An Investigation of Aerodynamic Heating to Spherically Blunted Cones at Angle of Attack," M.S. Thesis, George Washington Univ., Washington, DC, Aug. 1992.

[4]Shimshi, J. P., and Walberg, G. D., "An Investigation of Aerodynamic Heating to Spherically Blunted Cones at Angle of Attack," AIAA Paper 93-2764, July 1993.

[5]Weilmuenster, K. J., and Hamilton, H. H., "Calculations of Inviscid Flow over Shuttle-Like Vehicles at High Angles of Attack and Comparisons with Experimental Data," NASA TP-2103, May 1983.

[6]Weilmuenster, K. J., and Hamilton, H. H., "Computed and Experimental Surface Pressure and Heating on 70 Degree Sphere Cones," *Journal of Spacecraft and Rockets*, Vol. 24, No. 5, 1987, pp. 385–393.

[7]Cooke, J. C., "An Axially Symmetric Analogue for General Three-Dimensional Boundary Layers," R & M. No. 3200, British Aeronautical Research Council, 1961.

[8]Zoby, E. V., Moss, J. N., and Sutton, K., "Approximate Convective-Heating Equations for Hypersonic Flows," *Journal of Spacecraft and Rockets*, Vol. 18, No. 1, 1981, pp. 64–70.

[9]Hamilton, H. H., Millman, D. R., and Greendyke, R. B., "Finite-Difference Solution for Laminar or Turbulent Boundary Layer Flow over Axisymmetric Bodies with Ideal Gas, CF_4 or Equilibrium Air Chemistry," NASA TP-3271, Dec. 1992.

[10]Fay, J. A., and Riddell, F. R., "Theory of Stagnation Point Heat Transfer in Dissociated Air," *Journal of the Aeronautical Sciences* Vol. 25, No. 2, 1958, pp. 73–85, 121.

T. C. Lin
Associate Editor

Wind Tunnel Simulation of Multibooster Separation Trajectories of a Launch Vehicle

H. Sundara Murthy* and G. K. Suryanarayana*
National Aerospace Laboratories, Bangalore, India
and
R. Lochan,† A. E. Sivaramakrishnan,† and S. Pandian†
Vikram Sarabhai Space Center, Trivandrum, India

Introduction

LAUNCH vehicles often incorporate multiple strap-on boosters as a design feature to achieve enhanced performance goals. Titan III, Delta 1914, Ariane, and Long March 2C are some of the launch vehicles featuring such boosters numbering from two to nine. When the burnt-out boosters are ejected from the advancing core, no collision should occur between the separated parts and the rest of the launch vehicle. During this process, the aerodynamic forces and moments acting on the separating bodies play a crucial role, especially when separation takes place at a high dynamic pressure. Various workers in the past (e.g., Refs. 1 and 2) have used conventional captive trajectory systems for determining the trajectory of a body separating from a launch vehicle. In these tests, however, a single body was separated from the parent body.

In the present paper, wind-tunnel investigations undertaken to study the separation characteristics of four strap-on boosters simultaneously separating from the core of a launch vehicle are described. The emphasis is on presenting the overall approach adopted for the investigations, and only some typical data are included. Similar work to determine the trajectories of two strap-on boosters simultaneously separating from a launch vehicle is reported in Ref. 3. The problem was handled in two phases. Initially, tests were conducted to generate extensive data by placing the boosters at a series of preselected locations and orientations in a region around the core. These tests, called grid tests, provided the necessary aerodynamic input for the design of the ejection mechanism.

The second phase of testing was undertaken after finalizing the design of the ejection mechanism and was essentially meant to ascertain its adequacy for safe separation of the boosters. A novel technique called the semicaptive-trajectory technique (SECTT) was adopted to accurately determine the trajectories of the four separating boosters for the most critical combination of parameters. SECTT is a semimanual version of the automatic captive-trajectory technique and is especially suited to handle multiple separating bodies in an intermittent wind tunnel with short-duration testing.

In the SECTT, the first wind-tunnel run is conducted with the boosters in their unseparated (frozen) position, and aerodynamic loads on the separating boosters are measured. These data—along with other relevant parameters such as the mass-inertial properties of the booster, force-displacement history of the springs, etc.—are used to solve the Euler equations of motion for a short interval of time. This solution, which is carried out off line in a digital computer, gives the next position and orientation of each of the four boosters at the end of the integration period. The boosters are then manually moved to the new position and orientation, and the next test is carried out. Results from this test are utilized to obtain the subsequent position of the boosters. This step-by-step approach is continued till a description of the separation trajectories is obtained in the region of interest.

Received Jan. 24, 1994; revision received Sept. 27, 1994; accepted for publication Oct. 5, 1994.

*Scientist.

†Engineer.

Description of the Model and the Experimental Set-Up

Figure 1 shows a sketch of the launch-vehicle model. It features six strap-on boosters and two secondary-injection thrust-vector control (SITVC) rockets clustered around a core vehicle. The boosters numbered 1 to 4 are equipped with two pairs of spring housings each and are designed to separate simultaneously at the design Mach number of 3.1. The other two boosters and the SITVC tanks remain fixed to the core vehicle.

A special test rig was built for the present study. The rig features four independent articulated support mechanisms for each of the boosters and a central sting for supporting the core vehicle. The articulated mechanism permits six-degree-of-freedom positioning of each of the four boosters. Figure 2 shows a photograph of the model mounted on the rig in the 1.2-m trisonic blowdown wind tunnel at the National Aerospace Laboratories (NAL).

Simulation of Dynamics and Related Software

A very general six-degree-of-freedom rigid-body model was derived for the separating boosters, whereas the core vehicle was assumed to be under ideal control. A set of 12 simultaneous first-order differential equations for each of the boosters was developed, and numerical integration performed using a modified Euler approach. The forces included for analysis are gravity, aerodynamic forces, thrust, tail-off thrust, and the spring forces of the ejection mechanism.

Two types of trajectories were determined using the SECTT. In the first case, the trajectory computations were performed using the measured aerodynamic coefficients and nominal values of other relevant parameters. The trajectory so obtained is termed the nominal trajectory. In the other case (called the perturbed trajectory), magnitudes of some of the measured and other important parameters were perturbed by their estimated uncertainty values in such a way that the resulting trajectory would be most unfavorable from the point of view of collision.

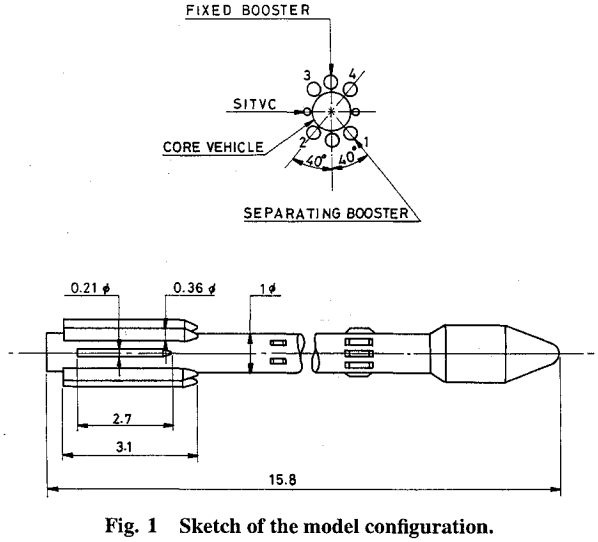

Fig. 1 Sketch of the model configuration.